

Article

Role of Precipitates on the Grain Coarsening of 20CrMnTi Gear Steel during Pseudo-Carburizing

Rui Zhang ¹, Qing Yuan ^{2,3,*}, En Tang ¹, Jiakuan Mo ², Zhicheng Zhang ³, Haijiang Hu ²  and Guang Xu ² 

¹ Department of Materials Engineering, Zhejiang Industry & Trade Vocational College, Wenzhou 325000, China; zhangrui@zjtc.edu.cn (R.Z.); tangen@zjtc.edu.cn (E.T.)

² State Key Laboratory of Refractories and Metallurgy, Wuhan University of Science and Technology, Wuhan 430081, China; m17363758032@163.com (J.M.); huhaijiang@wust.edu.cn (H.H.); xuguang@wust.edu.cn (G.X.)

³ Daye Special Steel Co., Ltd., Huangshi 435001, China; injector@126.com

* Correspondence: yuanqing@wust.edu.cn; Tel.: +86-159-9423-5997

Abstract: The carburizing period for tool steel could be significantly shortened by operating at a higher carburizing temperature. However, grain coarsening happens during the carburizing process, and then results in the deteriorated surface properties in 20CrMnTi gear steel, especially at an elevated carburizing temperature. The relationships between grain coarsening and the precipitates in the developed 20CrMnTi gear steel during pseudo-carburizing were established by microstructure characterization, precipitate analysis and in-situ observation to clarify the coarsening mechanism. The results manifested the Baker–Nutting orientation relationship between the (Ti, Mo)(C, N) particles and the matrix, and then testified to the redissolution and ripening of the (Ti, Mo)(C, N) precipitates pre-formed in the α phase during the carburizing. Coarsening in austenite grain during the carburizing process was mainly caused by the rapid redissolution and ripening of the (Ti, Mo)(C, N) precipitates, although this occurred in a very short pseudo-carburizing time. The area density of the dispersed unripe (Ti, Mo)(C, N) particles markedly decreased from 0.389% in as-hot rolled gear steel to 0.341%, and then from 0.279% in carburized steels at 970 and 980 °C, respectively. Additionally, the redissolution and ripening of the (Ti, Mo)(C, N) precipitates were accelerated by the elevated carburizing temperature of 980 °C, at which time the growing rate in austenite grains was 2.34 $\mu\text{m}/\text{min}$ during the prior 1 min (0.79 $\mu\text{m}/\text{min}$ during the prior 3 min at 970 °C). The temperature then decreased to 0.003 $\mu\text{m}/\text{min}$ in the subsequent carburizing process. The results obtained our current work reflected that the particles with excellent thermal stability should play important roles in the limitation of grain coarsening during the carburizing process.

Keywords: gear steel; carburizing; grain coarsening; precipitates; redissolution



Citation: Zhang, R.; Yuan, Q.; Tang, E.; Mo, J.; Zhang, Z.; Hu, H.; Xu, G. Role of Precipitates on the Grain Coarsening of 20CrMnTi Gear Steel during Pseudo-Carburizing. *Metals* **2023**, *13*, 1422. <https://doi.org/10.3390/met13081422>

Academic Editors: Andrii Kostryzhev and Koh-ichi Sugimoto

Received: 25 June 2023

Revised: 27 July 2023

Accepted: 7 August 2023

Published: 8 August 2023



Copyright: © 2023 by the authors. Licensee MDPI, Basel, Switzerland. This article is an open access article distributed under the terms and conditions of the Creative Commons Attribution (CC BY) license (<https://creativecommons.org/licenses/by/4.0/>).

1. Introduction

Gear steel is mainly used in the transmission parts of automobiles, construction machinery and machinery manufacturing [1–4]. High quality gear steel requires excellent toughness and wear resistance, especially for heavy load gear, which is usually made of carburized steel [5,6]. Carburizing, as an advanced heat treatment process, accelerates the infiltration of the carbon element into the surface of the metals depending on the element diffusion at a high temperature. Then, the hardness, abrasive resistance, and fatigue life of the gear surface are obviously enhanced to satisfy the adverse working conditions [7–9]. The heat treatment for carburized gear steel consists in quenching and tempering after surface carburizing [10–12]. The carburized gear steel presents good toughness and plasticity because of the low carbon content in the core, and the gear surface can be hardened to HRC58~62 after carburizing [13,14]. In order to improve the performance of carburized gear steel, the steel needs to have enough hardenability to obtain enough depth of the hardening layer. Furthermore, the steel should have a low tendency of grain growth at a high temperature to ensure

that the matrix grains remain small in the carburizing process over a long period of time. Grain refinement of carburized gear steel is usually achieved by adding a certain amount of microalloying elements, such as Al (aluminum), Ti (titanium), Nb (niobium), etc., to form microalloying carbonitrides in the steel to prevent grain growth during long periods of carburizing. These carbonitride compounds dissolve at a high temperature and precipitate at a low temperature. Under the action of thermal cycling or strain, the recrystallization, $\gamma \rightarrow \alpha$ phase transformation and the second phase precipitation process are affected by carbonitrides through the dissolution and precipitation mechanism of carbon and nitrogen compounds. Moreover, a series of secondary effects, such as grain refinement, precipitation enhancement, recrystallization control, and inclusion modification are produced. Finally, the microstructure and comprehensive properties of steel are improved [15–19]. The main effects of alloying elements in carburized gear steel are diverse, and can be summarized in three parts. Firstly, the resistance of austenite grain growth during heating is achieved by alloying elements. Secondly, the recrystallization and grain growth after recrystallization during rolling are inhibited by alloying elements. Lastly, the alloying elements provide an outstanding precipitation strengthening effect at a low temperature [20–24].

20CrMnTi steel, one of the most widely used types of commercial carburized gear steel in China, evolved from 18XTT steel, and its chemical compositions are mainly Cr-Mn-Ti series [25]. The distinguishing features of this steel are its high cleanliness, narrow hardenability and ultrafine grain. The ultrafine grain located at the carburized layer plays a determining role in the guarantee of excellent strength and hardness. The fine martensitic structure is obtained by the fine uniform austenite grain after quenching, which can noticeably improve the fatigue properties of the gear, and reduce the deformation of the gear after heat treatment. The relationship between surface grain size and the bending fatigue limit of carburizing steel obeys the Hall–Petch law, that is, the smaller the surface grain size, the higher the fatigue limit. A large number of experimental results show that the fatigue cracks propagate along the soft phase, and the fatigue cracks propagate along the network ferrite formed by the original austenitic grain boundary. Therefore, refining austenite is helpful to prevent the propagation of fatigue cracks.

However, a higher carburizing temperature is increasingly encouraged to shorten the carburizing time, and then increase efficiency. Unfortunately, grain coarsening often occurred in one self-developed 20CrMnTi steel at higher carburizing temperatures, although the temperature variation was very small. The carburized 20CrMnTi steel with coarsening grains could not be applied due to its aggravated mechanical properties. Therefore, it is necessary to investigate the grain coarsening mechanism at different carburizing temperatures during the carburizing process. In the present study, as-hot rolled 20CrMnTi steel and pseudo-carburized 20CrMnTi steels were used as the experimental steels. It should be pointed out that pseudo-carburizing refers to one heat treatment simulated material core, microstructure variations with temperature, and holding time without carburizing atmosphere. The characterization of the elaborated microstructure and observations of the precipitates were carried out to clarify the relationship between the precipitation and grain coarsening at different temperatures. In addition, in-situ observation of nucleation and the growth of austenite grains at different carburizing temperatures were performed. The elevated carburizing temperature achieved via the fabrication of 20CrMnTi gear steel will manifest great progress in the production process and commercial efficiency. The results of the present work will clarify the essence of grain coarsening at different carburizing temperatures, and then provide references for carburizing or chemical composition optimization of 20CrMnTi gear steel for industrial production.

2. Materials and Experimental Methods

A commercial 20CrMnTi gear steel (Daye Special Steel Co., Ltd., Huangshi, China) with a chemical composition of Fe-0.20C-0.25Si-0.99Mn-1.18Cr-0.02Ni-0.033Al-0.008V-0.056Ti-0.04Mo-0.006W-0.009P-0.016S (wt%) was used as the experimental steel. Figure 1a presents the pseudo-carburizing process. Cylindrical specimens with a diameter of 10 mm and

height of 8 mm were finishing machined before pseudo-carburizing. Three different steels were prepared, including as-hot rolled, which were pseudo-carburized at 970 °C and 980 °C for 4 h. After pseudo-carburizing, the two steels were quenched in the room temperature water to preserve the morphology and size of the parent austenite grains. The microstructure observations were performed on a Nova 400 Nano field emission scanning electron microscope (FE-SEM, FEI Co., Hillsboro, OR, USA) and a ZEISS optical microscope (OM, ZEISS, Oberkochen, Germany). The parent austenite grains were distinguished using a saturated water solution of picric acid, cream shampoo, and hydrochloric acid solution. The grain sizes of the parent austenite grains were measured based on 4–6 images and 35–55 grains. Carbon replicas were prepared to analyze the precipitates using a JEM-2100F transmission electron microscope (TEM, JEOL, Tokyo, Japan) equipped with an energy-dispersive spectrometer (INCA-EDS) operating at 200 kV. The size and area density of the precipitates were determined based on the number of precipitates with the software Image Pro Plus 6.0. Additionally, the hardness of steels pseudo-carburized at 970 °C and 980 °C were measured on an HV-1000 Vickers hardness tester (Laizhou Dechuan test Instrument Co., Ltd., Lanzhou, China). The average of the six measurements was used as the final hardness of the pseudo-carburized steels.

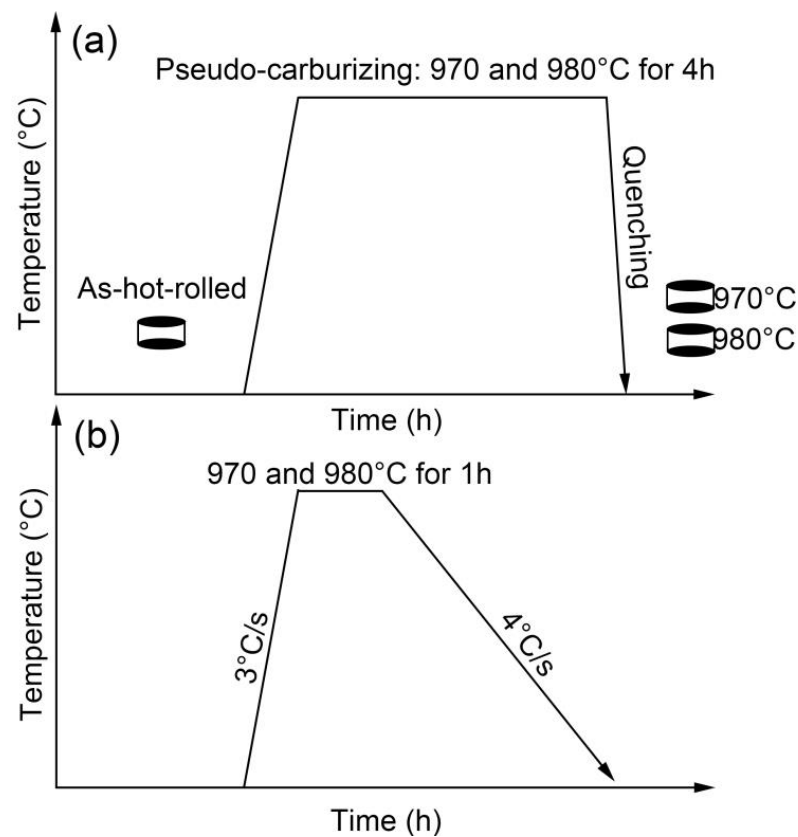


Figure 1. (a) Pseudo-carburizing process and (b) in-situ observation with different pseudo-carburizing temperatures.

In order to reflect the austenite grain nucleation and growth in real time during the pseudo-carburizing process, in-situ observation was performed with a VL2000DX laser scanning confocal microscope (LSCM) (Lasertec, Yokohama, Japan) with different pseudo-carburizing temperatures of 970 and 980 °C (Figure 1b). Cylindrical specimens for the in-situ observation were finishing machined to $5 \times 5 \text{ mm}^2$ (diameter and height), and then opposite sides of all specimens were sanded and polished. It was noted that the pseudo-carburizing time of 1 h was employed in view of the safety protection of experimental equipment.

3. Results

3.1. Microstructure

Figure 2a–c shows the morphologies of as-hot rolled and pseudo-carburized steels quenched at 970 and 980 °C. The initial microstructure before pseudo-carburizing was polygonal ferrite (F) and pearlite (P). Quenching lath martensite (M) were obtained after pseudo-carburizing. Figure 2d–f displays the parent austenite grains for the two pseudo-carburized steels and their grain size distributions. The average size of the parent austenite grain in pseudo-carburized steel at 970 °C was $29.37 \pm 4.11 \mu\text{m}$ smaller than that in the pseudo-carburized steel at 980 °C ($32.89 \pm 4.52 \mu\text{m}$). It was found that most of the parent austenite grains were of homogeneous grain size in the steel pseudo-carburized at 970 °C, whereas the grain size distribution in the steel pseudo-carburized at 980 °C migrated to a relatively larger scale. Furthermore, some coarsened grains (indicated by arrows) appeared in the steel pseudo-carburized at 980 °C. The coarse austenite grains demonstrated that the ultimate carburizing temperature for this 20CrMnTi gear steel was 970 °C. The carburizing temperature for this 20CrMnTi gear steel was elevated to hardness at 980 °C.

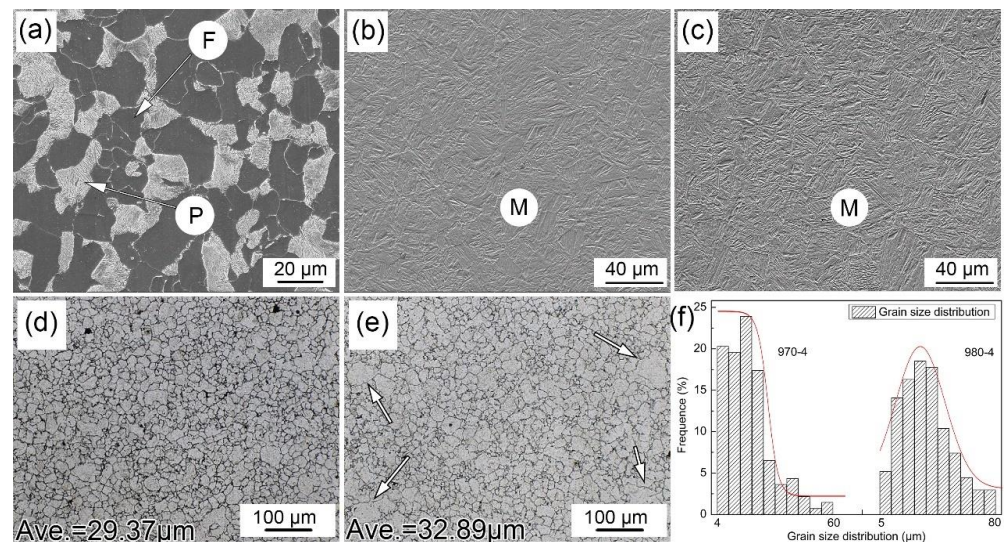


Figure 2. Morphologies of (a) as-hot rolled specimen, (b) pseudo-carburized steels quenched at 970 °C; (c) pseudo-carburized steels quenched at 980 °C, (d) parent austenite grains at 970 °C; (e) parent austenite grains at 980 °C and (f) its size distribution.

3.2. Hardness

Table 1 shows the measurement result of hardness in the pseudo-carburized steels quenched at 970 and 980 °C. The pseudo-carburized steels quenched at 970 °C yielded a hardness of $497.0 \pm 23.2 \text{ Hv}$ higher than that of the steels quenched at 980 °C (479.7 ± 18.7). The elevated hardness in pseudo-carburized steel at 970 °C might be explained by its fewer coarsening grains; thus, the quenching martensite would be refined.

Table 1. Hardness of the pseudo-carburized steels quenched at 970 and 980 °C.

| Steel | 1 | 2 | 3 | 4 | 5 | 6 | Average |
|----------------------------|-------|-------|-------|-------|-------|-------|------------------|
| carburized steel at 970 °C | 502.4 | 498.6 | 511.1 | 487.7 | 482.3 | 499.7 | 497.0 ± 23.2 |
| carburized steel at 980 °C | 476.2 | 475.4 | 489.4 | 491.2 | 474.3 | 471.8 | 479.7 ± 18.7 |

3.3. Precipitations

The precipitates' morphologies, ranging from as-hot rolled steel to the pseudo-carburized steels at 970 and 980 °C, are exhibited in Figure 3. Different magnifications of the images were used to better highlight the precipitate distribution. These precipitates were determined to

be the (Ti, Mo)(C, N) precipitates using energy spectrum analysis, and following selected area electron diffraction pattern. It can be seen that a large amount of micro/nano scale (Ti, Mo)(C, N) precipitates were found in the as-hot rolled steel, in which few abnormal precipitates with large sizes were captured. The size and area density for micro/nano scale precipitates (excluding the excessively large precipitates) in as-hot rolled steel were determined to be 3.4–28.7 nm and 0.389%, respectively. However, the volume fraction of micro/nano scale precipitates radically decreased in the pseudo-carburized steels. Additionally, the volume fraction of relatively larger (Ti, Mo)(C, N) particles increased, especially in the pseudo-carburized steels at 980 °C. The size of the (Ti, Mo)(C, N) particles in pseudo-carburized steels at 970 and 980 °C were determined to be 4.9–34.4 nm and 6.8–52.1 nm, respectively, and the area densities were 0.341% and 0.279%, respectively. In addition, it was concluded from the energy spectrum analysis that the content of the C element was higher than that of the N element in three steels. Moreover, the content of the C element in the (Ti, Mo)(C, N) precipitates gradually decreased from the (Ti, Mo) $C_{0.90}N_{0.10}$ precipitates in as-hot rolled steel to the (Ti, Mo) $C_{0.72}N_{0.28}$ precipitates, and then the (Ti, Mo) $C_{0.64}N_{0.36}$ precipitates in the pseudo-carburized steels at 970 and 980 °C.

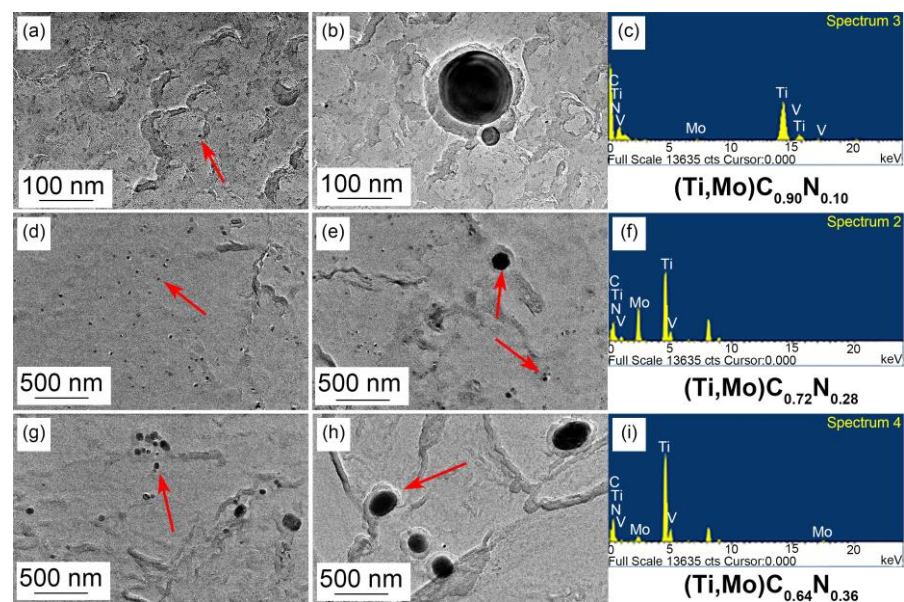


Figure 3. Precipitates in (a–c) as-hot rolled and pseudo-carburized steels at (d–f) 970 °C and (g–i) 980 °C with corresponding energy spectrum analysis (Typical carbides were shown by red arrows).

Figure 4 exhibits the high-resolution morphology of the (Ti, Mo)(C, N) particles in the pseudo-carburized steel at 980 °C. It was found that the size of the (Ti, Mo)(C, N) particles exceeded 20 nm, which led to the loss of effective precipitation strengthening and a fine grain strengthening role. The high-resolution lattice phase of the (Ti, Mo)(C, N) particles was obtained in Figure 4c by inverse Fast-Fourier Transformation (FFT). The lattice constant of the (Ti, Mo)(C, N) particles was calculated to be 0.414 nm closed to lattice constant of ferrite multiplied by $\sqrt{2}$ based on the (200) plane spacing of 0.207 nm. Therefore, the Baker–Nutting orientation relationship between the lattice planes of $(200)_{\alpha}$ and $(011)_{(Ti,Mo)(C,N)}$ was determined according to $(002)_{(Ti,Mo)(C,N)} // (002)_{\alpha}$ and $[-110]_{(Ti,Mo)(C,N)} // [010]_{\alpha}$ [26–28]. Consequently, it can be concluded that these (Ti, Mo)(C, N) particles mainly precipitated in the α phase during the cooling process after hot rolling. Thus, it was inferred that these (Ti, Mo)(C, N) particles with relative large size had been matured by the particles' redissolution.

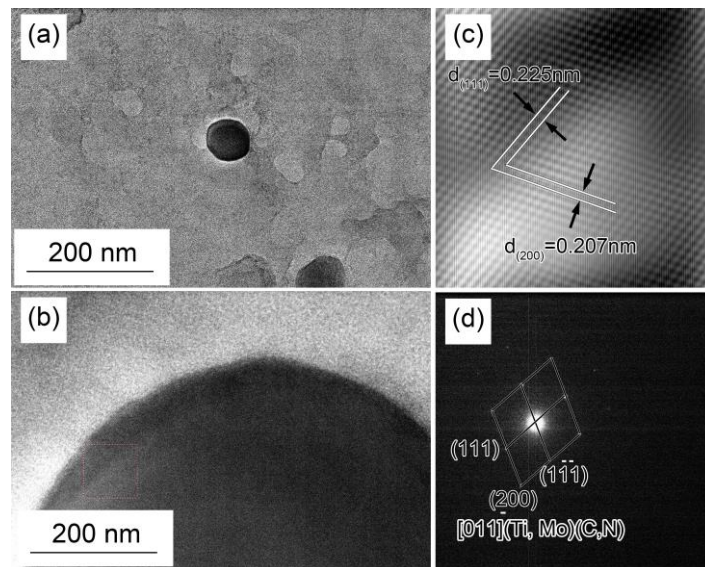


Figure 4. (a,b) High-resolution morphology of (Ti, Mo)(C, N) carbide and (c) its high-resolution lattice phase and (d) diffraction calibration.

3.4. In-Situ Observation

Figure 5 displays the austenitizing processes of the steels pseudo-carburized at 970 and 980 °C, respectively. The grain boundaries (GB) of pearlite and ferrite emerged at about ~530 °C during the heating stage due to the thermal etching effect (Figure 5a,d). In addition, some rare precipitates could be found in the matrix. The γ GBs are revealed gradually at ~745 °C around the GB of pearlite and ferrite as the temperature rises (Figure 5b,e). The volume fraction of the emerged precipitates increased with the increasing temperature. It was noted that most nano-scale precipitates (without coarsening) were inconspicuous due to the limited magnification of in-situ observation. Apparent austenite grains accompanied by precipitates were observed at the pseudo-carburizing temperatures of 970 and 980 °C (Figure 5c,f).

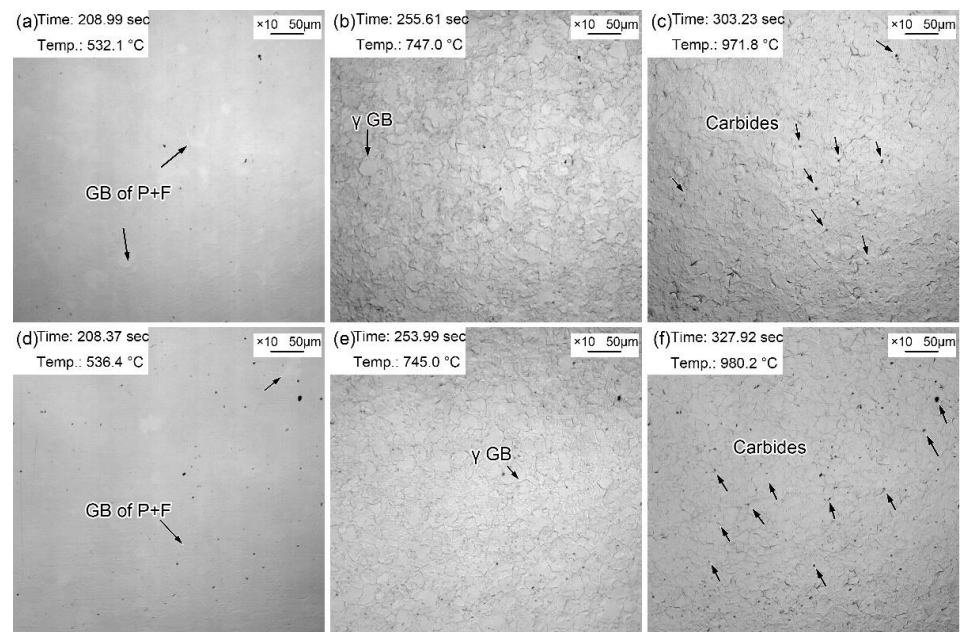


Figure 5. Austenitizing processes during pseudo-carburizing at (a–c) 970 °C and (d–f) 980 °C.

The variation of austenite grains during the prior 1–10 min of the pseudo-carburizing process with an interval of 1 min at 970 °C were recorded in Figure 6. The γ GBs became more and more legible due to the continuous thermal etching effect with the holding time. It was surprising to find the abnormal grain growth (marked by arrows) in austenite grains at a holding time of ~3 min. The volume fraction of uniform austenite grains with a small size decreased with the holding time, while enhanced grain coarsening was increasingly manifested (shown by rectangles). Furthermore, the dimension of these visible precipitates became larger with the holding time. More importantly, the volume fraction of visible precipitates increased with the holding time as well. It is inferred that the redissolution accompanied by the ripening of the precipitated (Ti, Mo)(C, N) particles happened during the pseudo-carburizing process. The random appearance of coarsening austenite grains was caused by the sufficient redissolution of small (Ti, Mo)(C, N) precipitates with poor chemical stability in critical size. More and more small-size activated (Ti, Mo)(C, N) precipitates dissolved, leading to the better chemical stability in these visible precipitates.

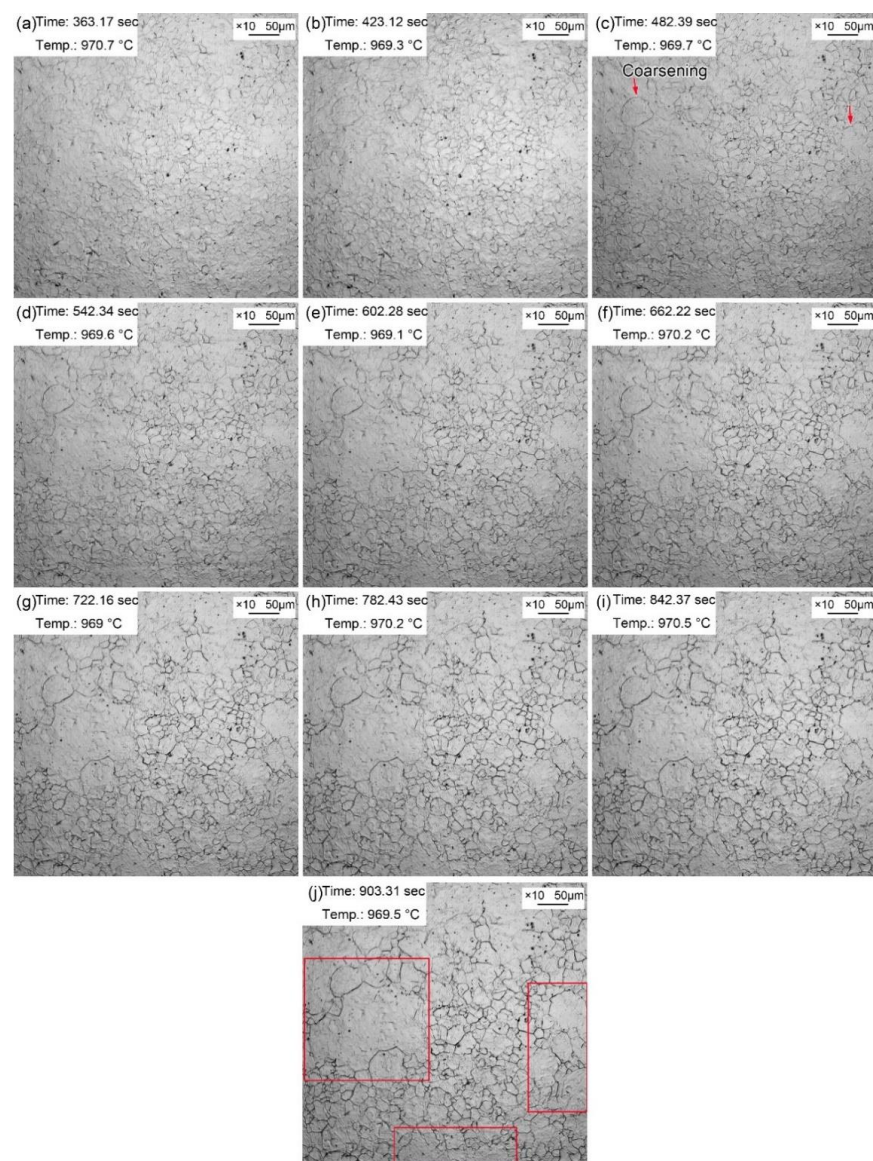


Figure 6. Variation of austenite grains during the prior (a–j) 1–10 min of pseudo-carburizing process with an interval of 1 min at 970 °C.

Figure 7 exhibits the variation of austenite grains during the prior 1–10 min of the pseudo-carburizing process with an interval of 1 min at 980 °C. It was interesting to discover

that the abnormal grain growth (marked by arrows) occurred at the prior 1 min, presenting advanced redissolution and the ripening of the precipitated (Ti, Mo)(C, N) particles at a higher pseudo-carburizing temperature. In addition, the volume fraction of the coarsening austenite grains markedly increased at 980 °C. Additionally, few fine austenite grains were observed as those before pseudo-carburizing. Moreover, the amount of (Ti, Mo)(C, N) precipitates that remained visible became greater compared with those in the pseudo-carburized steel at 970 °C. Results suggested that the minor elevated temperature prompted the redissolution and ripening of the precipitated (Ti, Mo)(C, N) particles. Likewise, it also manifested that the pseudo-carburizing temperature played a crucial role in the grain coarsening compared to the holding time during the pseudo-carburizing process.

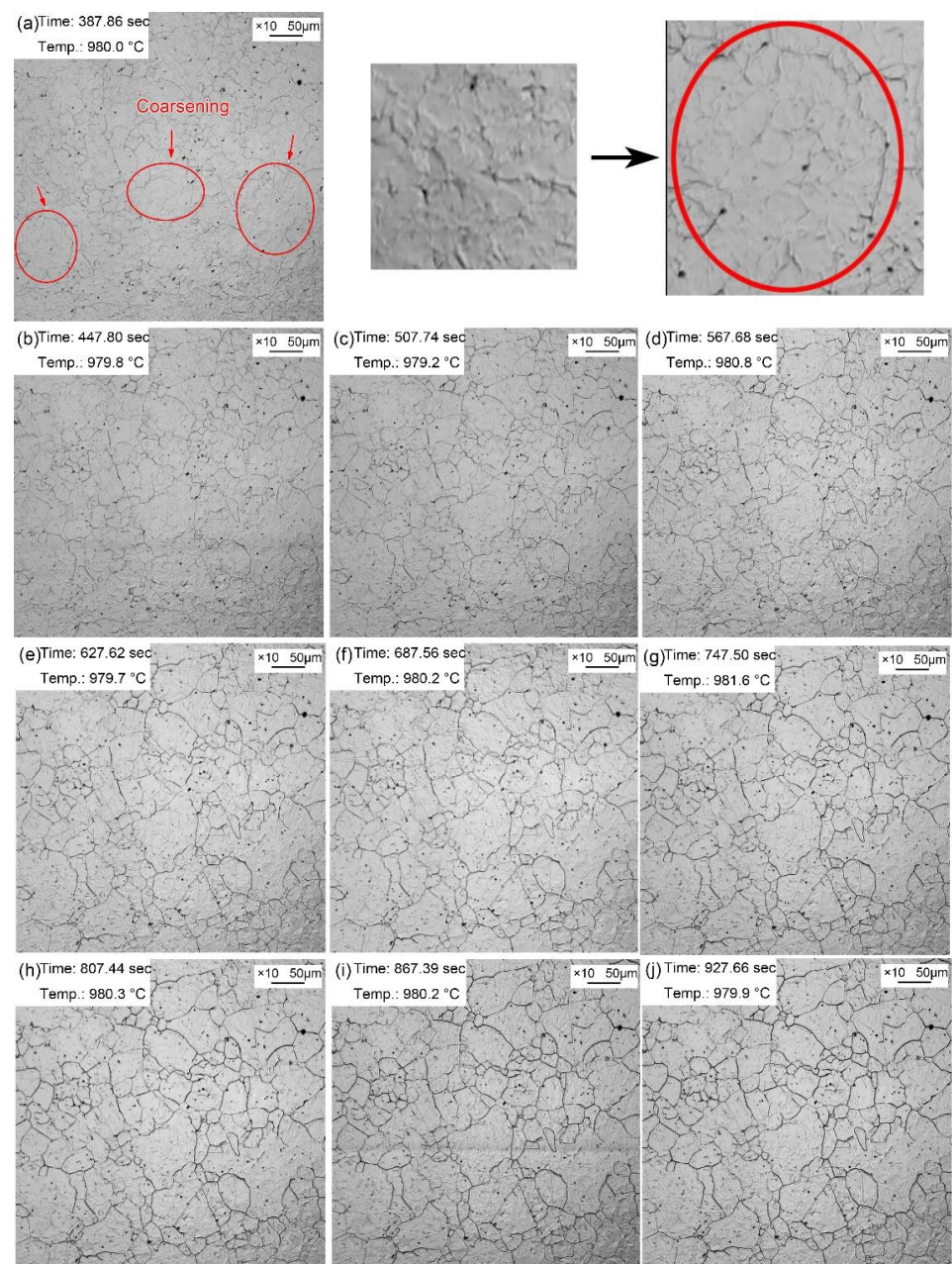


Figure 7. Variation of austenite grains during the prior (a–j) 1–10 min of pseudo-carburizing process with an interval of 1 min at 980 °C.

Morphology evolutions of austenite grains and precipitates at the subsequent holding time of 20–60 min in the pseudo-carburized steel at 970 °C are displayed in Figure 8.

Apparent grain growth was observed from a holding time of 20 min to 60 min (labelled by rectangle), and the volume fraction of fine and homogeneous austenite grains as those before pseudo-carburizing further decreased. The growth mechanisms of migration in austenite grain boundaries and the consolidation by many small grains were prominent in the grain coarsening. In addition, the coarsening (Ti, Mo)(C, N) precipitates became more arresting after 60 min of pseudo-carburizing, testifying to the drastic redissolution and ripening of the precipitated (Ti, Mo)(C, N) particles.

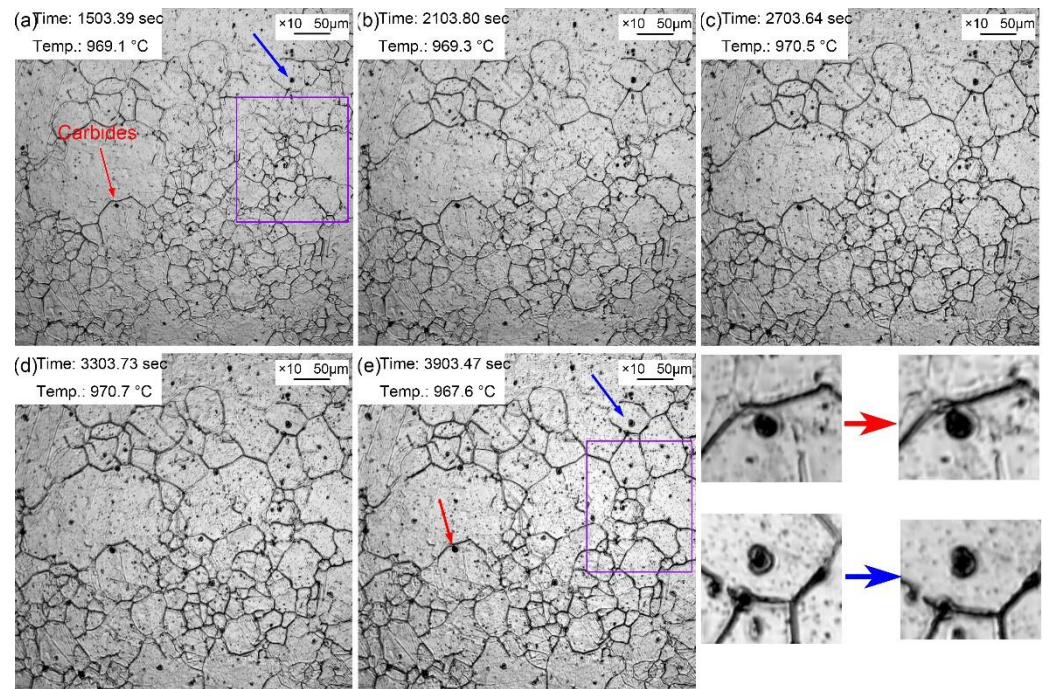


Figure 8. Morphology of austenite grains and precipitates at holding time of (a–e) 20–60 min in the pseudo-carburized steel at 970 °C.

Figure 9 shows the morphology evolutions of austenite grains and precipitates at the subsequent holding time of 20–60 min in the pseudo-carburized steel at 980 °C. Similar coarsening in grains and (Ti, Mo)(C, N) precipitates synchronously appeared. The volume fraction of fine and homogeneous austenite grains as those before pseudo-carburizing further decreased, and was even smaller than those at 970 °C. It was strongly demonstrated from in-situ observation that the fine (Ti, Mo)(C, N) precipitates dissolved and caused the maturation of other large size precipitated particles when pseudo carburizing temperature reached a certain value, and then accelerating the coarsening of parent austenite grains. Consequently, from the perspective of component optimization, the weight% of Ti and Mo in the developed 20CrMnTi gear steel should be designed to ensure better thermal stability in these (Ti, Mo)(C, N) particles at higher pseudo-carburizing temperatures.

Martensite transformations in the two steels during the cooling stage after pseudo-carburizing at 970 and 980 °C are shown in Figure 10. The M_s temperatures for the two steels were determined to be 506.6 °C and 537.7 °C, respectively. The increased M_s temperature for the pseudo-carburized steel at 980 °C might be caused by their relatively larger austenite grains which provided slightly feeble phase transition resistance on the martensite transformation. More martensite appeared with the decreasing temperature. However, martensite laths preferentially formed within the large austenite grains as well, although in the same steel. These asynchronous martensite transformations in the large and relatively small austenite grains were also caused by the different phase transition resistance introduced by its different strengths [29]. Besides, the different fluctuations in the structure and chemical composition affected the nucleation of martensite as well.

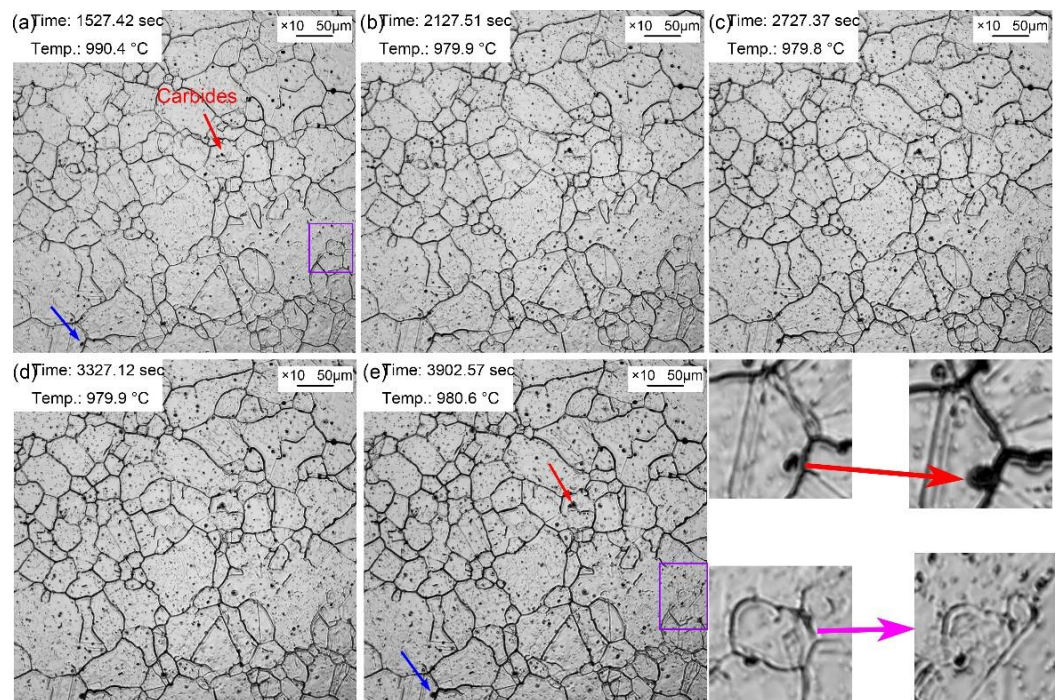


Figure 9. Morphology of austenite grains and precipitates at holding time of (a–e) 20–60 min in the pseudo-carburized steel at 980 °C.

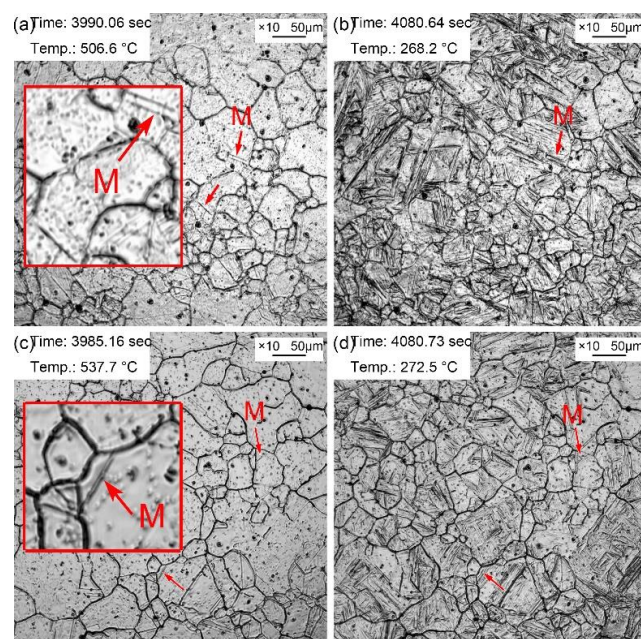


Figure 10. Martensite transformations in the two steels during cooling stage after pseudo-carburizing at (a,b) 970 °C and (c,d) 980 °C.

4. Discussion

The quantitative results of the size and area density of (Ti, Mo)(C, N) particles manifested the redissolution and ripening of some micro/nano scale (Ti, Mo)(C, N) precipitates during the carburizing process (Figure 3). Additionally, the redissolution and ripening for the (Ti, Mo)(C, N) precipitates became more drastic at 980 °C. Firstly, some (Ti, Mo)(C, N) precipitates redissolved in the matrix due to the increased temperature according to the formula for solid solubility product. Moreover, since the solute concentration around the

small particles was greater than that around the large particles, the solute atoms will diffuse from the small particles to the large particles, resulting in the dissolution of small-size precipitates and the growth of large precipitates [30]. Therefore, the fine (Ti, Mo)(C, N) precipitates gradually redissolved and large-size (Ti, Mo)(C, N) particles continuously formed under the long time carburizing process when the pseudo-carburizing temperature was high. The solid solubility product of the (Ti, Mo)C particles was large; thus, the content of the C element that redissolved into the matrix increased with the temperature. Nevertheless, the content of the redissolved N element gradually decreased with the increased pseudo-carburizing temperature due to the small solid solubility product of nitrides. The ratio variation of the C and N elements in the (Ti, Mo)(C, N) precipitates strongly proved the particles' redissolution during the pseudo-carburizing process.

The obvious coarsening of austenite grains in the pseudo-carburized steel at 980 °C was related to the redissolved (Ti, Mo)(C, N) precipitates. Firstly, the atomic size of Ti was quite different from that of Fe, so it had a certain solute atom dragging effect. The migration of the grain boundaries can be prevented when a large number of solute atoms such as Ti were reconcentrated on grain boundaries or sub-grain boundaries; thus, recrystallization was inhibited as well. In addition, the (Ti, Mo)(C, N) particles preferentially precipitated at grain boundaries and dislocation lines, which could pin the austenite grain boundaries and prevented austenite grain growth. The essence of the austenite grain growth was the migration of the grain boundaries. The grain boundaries tended to bend when contacting the (Ti, Mo)(C, N) precipitates, thereby increasing the surface energy. Only when the thermal activation energy was greater than the increase in surface energy could the (Ti, Mo)(C, N) precipitates be cut or bypassed by grain boundaries. Therefore, the (Ti, Mo)(C, N) precipitates significantly slowed down the austenite formation rate and effectively prevented the grain growth. The pinning-solving criterion of grain boundary in steel is presented in Equation (1) [30]:

$$D_c \leq \frac{\pi d}{6f} \left(\frac{3}{2} - \frac{2}{Z} \right) \quad (1)$$

where D_c is the critical average equivalent diameter of grains which can be effectively pinned, d is the average diameter of the second phase particle, f is the volume fraction of the second phase particle, and Z is the factor of grain size heterogeneity which equals the ratio of the maximum and average grain size. It reflects that in order to ensure the pinning effect, the number of the (Ti, Mo)(C, N) precipitates must be sufficient, and its average size was small enough. The volume fraction of the fine and dispersed (Ti, Mo)(C, N) particles decreased significantly when the pseudo-carburizing temperature was 980 °C, at which time the volume fraction of the large size (Ti, Mo)(C, N) precipitates increased, leading to the weakening pinning effect on the grain boundary migration. Hence, the grain boundaries of some austenite grains expanded outward, resulting in austenite grain coarsening.

Ostwald first studied the variation of precipitated particle size in a dilute solution [30]. The widely used theoretical formula for calculating the Ostwald ripening law of spherical particles uniformly precipitated in matrix under diffusion control is given in Equation (2) [30]:

$$d_t^3 = d_0^3 + \frac{64D\sigma V_s^2 C_0}{9RTV_m C_p} t = d_0^3 + m^3 t \quad (2)$$

where d_0 is the initial grain size of precipitates, and d_t is the average size of the precipitates after time t . D is the diffusion coefficient of the controlling element M (such as Ti) in the matrix; σ is the interface energy between the precipitates and the matrix; V_s is the molar volume of the precipitates; V_m is the molar volume of the matrix; C_0 and C_p are the equilibrium atomic concentration of the controlling element M (such as Ti) in the matrix and in the precipitates, respectively; R is the molar gas constant and T is the absolute

temperature. m is defined as the coarsening rate of precipitates ($\text{nm}/\text{sec}^{1/3}$) and it could be calculated by Equation (3) as follows:

$$m = \left(\frac{64D\sigma V_S^2 C_0}{9RTV_m C_p} \right)^{1/3} \quad (3)$$

It could be inferred from the relationships between m and T & t that the pseudo-carburizing temperature seriously affected the coarsening rate of precipitates when m^3 in analogy with the slope of the equation. It may be explained by the exponential relationship between the redistribution of chemical elements in the (Ti, Mo)(C, N) precipitates with temperature. Additionally, the migration and combining of elements also expressed a positive correlation with temperature. The small temperature oscillation causing the coarsening austenite grains also yielded the larger stimulated effect on the grain boundary migration.

The average size variations of austenite grains and its growth rates starting from the appearance of austenite in the two steels pseudo-carburized at 970 and 980 °C are displayed in Figure 11. All the austenite grains were counted as far as possible under the fixed field of view by in-situ observation. The austenite grains violently grew up in the prior 10 min during the pseudo-carburizing process. Therefore, the variation curves of average grain sizes presented apparent two different stages showing the rapid increase and near-stable state in size. The abnormal grain growth in austenite grains was caused by the decreased pinning effect to the GBs of the ripened (Ti, Mo)(C, N) particles (Figure 6i). The near-stable state in grain size may be explained by the gradually disappeared pinning effect of the ripening (Ti, Mo)(C, N) particles, and the stimulation to the migration of grain boundaries were not further enhanced due to the unchanged temperature. The average size of austenite grains in the steel pseudo-carburized at 970 °C was still smaller than that at 980 °C. Consequently, both the precipitation and grain refinement strengthening effects were weakened due to the ripened (Ti, Mo)(C, N) particles and then coarsened grains at 980 °C, resulting in the lower hardness of 479.7 ± 18.7 Hv. On one hand, the higher carburizing temperature of 980 °C led to the coarsened austenite grains and then the martensitic laths. The strength or hardness of martensite decreased with the dimension of martensitic laths. On the other hand, the ripened (Ti, Mo)(C, N) particles without any precipitation strengthening effect acting as inclusions deteriorated the strength. The surface hardness of carburized gear steel should be improved by the carburizing process; however, the inapposite higher carburizing temperature sacrificed the precipitation and grain refinement strengthening effects in the developed 20CrMnTi gear steel.

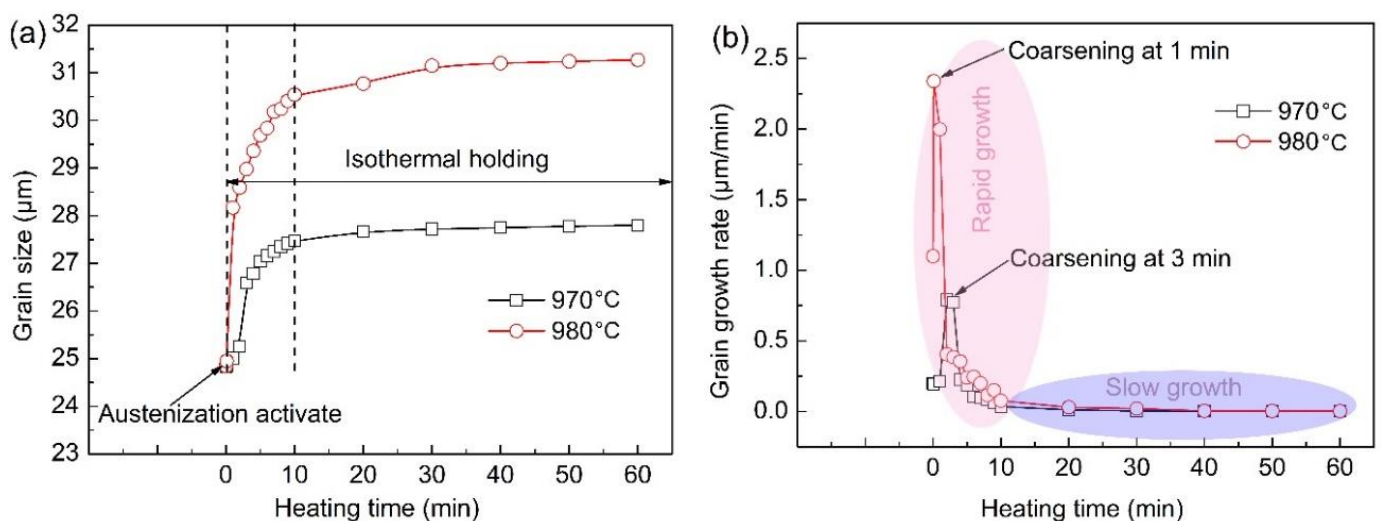


Figure 11. (a) Average size variations of austenite grains and (b) its growth rates in the two steels pseudo-carburized at 970 and 980 °C.

Moreover, the increase of average size in the steel pseudo-carburized at 970 °C was inferior to that observed at 980 °C. The final average sizes of austenite grains were both smaller than those obtained in Figure 2 because of the short pseudo-carburizing time. The maximum growth rates in austenite grains appeared at pseudo-carburizing times of 1 and 3 min, respectively, in the steels pseudo-carburized at 980 and 970 °C. In a word, the growing tendency in austenite grain was easy to be motivated by the rapid redissolution and ripening of the precipitated (Ti, Mo)(C, N) particles at a higher pseudo-carburizing temperature, although in a very short pseudo-carburizing time. The poor thermostability of the (Ti, Mo)(C, N) particles in this developed 20CrMnTi gear steel induced the drastic grain coarsening at 980 °C. Therefore, the thermostability of the (Ti, Mo)(C, N) particles should be further improved by chemical composition redesign to satisfy the higher pseudo-carburizing temperature.

5. Conclusions

- (1) The ratio variation of the C and N elements in the (Ti, Mo)(C, N) precipitates from as-hot rolled steel to the pseudo-carburized steels at 970 and 980 °C, as well as the Baker–Nutting orientation relationship between particles and the matrix, both proved the particles' redissolution during the pseudo-carburizing process.
- (2) The rapid redissolution and ripening of the (Ti, Mo)(C, N) precipitates yielded the coarsening austenite grain during the carburizing process. Furthermore, the redissolution and ripening of the (Ti, Mo)(C, N) precipitates were generated by increasing the pseudo-carburizing temperature.
- (3) The pseudo-carburizing temperature played an important role compared to the holding time on the grain coarsening, thus the grain coarsening happened at the prior 1 min during the pseudo-carburizing process at 980 °C with a maximum growing rate of 2.34 µm/min. The growing rate of austenite grains decreased to be 0.79 µm/min, corresponding to the sharp coarsening at 970 °C.
- (4) The weight% of Ti and Mo in the developed 20CrMnTi gear steel should be designed to ensure better thermal stability at higher pseudo-carburizing temperatures from the perspective of component optimization.

Author Contributions: Conceptualization, R.Z. and Q.Y.; methodology, E.T. and J.M.; validation, Z.Z., H.H. and G.X.; formal analysis, R.Z.; investigation, E.T.; resources, Q.Y.; data curation, R.Z. and E.T.; writing—original draft preparation, R.Z.; writing—review and editing, Q.Y. and G.X.; supervision, Z.Z.; project administration, Q.Y.; funding acquisition, Q.Y. and R.Z. All authors have read and agreed to the published version of the manuscript.

Funding: This research was funded by the National Natural Science Foundation of China (NSFC) (No. 52004193), the China Postdoctoral Science Foundation (2022M710596) and the Talent Foundation of Zhejiang Industry & Trade Vocational College.

Data Availability Statement: Not applicable.

Acknowledgments: The authors gratefully acknowledge the 20CrMnTi gear steel provided by Daye Special Steel Co., Ltd.

Conflicts of Interest: The authors declare no conflict of interest.

References

1. Vella, H. Gear up for green steel. *Eng. Technol.* **2022**, *17*, 47–55. [[CrossRef](#)]
2. Ren, Z.D.; Li, B.Z.; Zhou, Q.Z.; Hou, R.D.; Zhang, Y.W. Optimization of high-speed grinding parameters for anti-fatigue performance of 20CrMnTi steel. *Int. J. Adv. Manuf. Technol.* **2022**, *122*, 3565–3581. [[CrossRef](#)]
3. Chen, W.; He, X.F.; Yu, W.C.; Shi, J.; Wang, Q.; Yao, K.F. Characterization of the microstructure and hardness of case-carburized gear steel. *Micron* **2021**, *144*, 103028. [[CrossRef](#)]
4. Fuchs, D.; Tobie, T.; Stahl, K. Challenges in determination of microscopic degree of cleanliness in ultra-clean gear steels. *J. Iron Steel Res. Int.* **2022**, *29*, 1583–1600. [[CrossRef](#)]
5. Shen, W.J.; Cheng, G.G.; Hou, Y.Y.; Li, Y.; Zhan, X.L.; Liu, J.J. Effects of the cooling rate and recovery temperature on the growth of AlN precipitates in gear steel. *Steel Res. Int.* **2022**, *93*, 2200281. [[CrossRef](#)]

6. Mehtap, A.; Cem, O.A.; Kartal, S.G.; Timur, S. Investigation on structural and tribological properties of borided gear steel after phase homogenization. *Surf. Coat. Technol.* **2022**, *429*, 127967.
7. Chen, D.F.; Zhu, J.Z.; Liu, H.J.; Wei, P.T.; Mao, T.Y. Experimental investigation of the relation between the surface integrity and bending fatigue strength of carburized gears. *Sci. China Technol. Sci.* **2023**, *66*, 33–46. [[CrossRef](#)]
8. Mathews, A.; Farahani, H.; Sietsma, J.; Petrov, R.H.; Mecozzi, M.G.; Santofimia, M.J. Microstructures in a carburized steel after isothermal pearlitic treatment. *J. Mater. Res. Technol.* **2023**, *160*, 66–75. [[CrossRef](#)]
9. Hong, Y.; Sun, C.; Xiu, S.C.; Xu, C.W.; Ma, L.; Zou, X.N. Strengthening surface generation mechanism of carburizing-assisted grinding. *Tribol. Int.* **2003**, *180*, 108300. [[CrossRef](#)]
10. Shi, L.; Cui, X.F.; Li, J.; Jin, G.; Liu, J.N.; Tian, H.L. Improving the wear resistance of heavy-duty gear steels by cyclic carburizing. *Tribol. Int.* **2022**, *171*, 107576. [[CrossRef](#)]
11. Lisle, T.J.; Little, C.P.; Aylott, C.J.; Shaw, B.A. Bending fatigue strength of aerospace quality gear steels at ambient and elevated temperatures. *Int. J. Fatigue* **2022**, *164*, 107125. [[CrossRef](#)]
12. Zhang, G.Q.; He, X.F.; Zhang, Q.Z.; Wang, W.J.; Wang, M.Q. Comparison of microstructure and heat treatment distortion of gear steels with and without Nb addition. *J. Iron Steel Res. Int.* **2021**, *28*, 488–495. [[CrossRef](#)]
13. Wu, J.Z.; Wei, P.T.; Liu, H.J.; Zhang, X.H.; He, Z.Q.; Deng, G.Y. Evaluation of pre-shot peening on improvement of carburizing heat treatment of AISI 9310 gear steel. *J. Mater. Res. Technol.* **2022**, *18*, 2784–2796. [[CrossRef](#)]
14. Mengaroni, S.; Bambach, M.D.; Cianetti, F.B. Strengthening improvement on gear steels. *Steel Res. Int.* **2016**, *87*, 608–613. [[CrossRef](#)]
15. Parvinzadeh, M.; Karganroudi, S.S.; Omid, N.; Barka, N.; Khalifa, M. A novel investigation into edge effect reduction of 4340 steel spur gear during induction hardening process. *Int. J. Adv. Manuf. Technol.* **2021**, *113*, 605–619. [[CrossRef](#)]
16. Carvalho, A.A.; Rego, R.R.; Colombo, T.C.A.; Oliveira, A.L.R.D.; Righetti, V.A.N.; Thim, G.P.; Galdino, R.S.; Pinto, J.A.C.C.; Freese, S.H.; Coromberk, C.C.E. Surface integrity evolution of Nb-Ti microalloyed steels along the gear manufacturing chain. *Int. J. Mech. Sci.* **2021**, *212*, 106807. [[CrossRef](#)]
17. Navin, R.I.; Babu, P.D.; Marimuthu, P.; Phalke, S.S. Distribution of residual compressive stresses in induction hardened steel gears: Effect of parameters on distortion, hardness and phase composition. *Met. Sci. Heat Treat.* **2021**, *63*, 449–455. [[CrossRef](#)]
18. Zhang, Y.F.; Fang, C.Y.; Huang, Y.F.; Guo, W.L.; Xing, Z.G.; Wang, H.D.; Zhang, Z.N. Enhancement of fatigue performance of 20Cr2Ni4A gear steel treated by pulsed magnetic treatment: Influence mechanism of residual stress. *J. Magn. Magn. Mater.* **2021**, *540*, 168327. [[CrossRef](#)]
19. Tang, H.Y.; Yang, M.S.; Men, W.J.; Lan, P.; Wang, C. Hot deformation behaviour and microstructure of a high-alloy gear steel. *Mater. Sci. Technol.* **2018**, *34*, 1228–1238. [[CrossRef](#)]
20. Ahn, S.H.; Heo, J.; Kim, J.; Hwang, Cho, I. The effect of baking heat treatment on the fatigue strength and life of shot peened 4340M landing gear steel. *Materials* **2020**, *13*, 5711. [[CrossRef](#)]
21. Barglik, J.; Ducki, K.; Kuc, D.; Smagór, A.; Smalcerz, A. Hardness and microstructure distributions in gear wheels made of steel AISI 4340 after consecutive dual frequency induction hardening. *Int. J. Appl. Electrom.* **2020**, *63*, S131–S140. [[CrossRef](#)]
22. Ma, Q.; Zhao, X.; Meng, D.; Dong, C.; Hou, Z.; Misra, R.D.K. Microstructure and hardness evolution during deformation near Ae(3) in a Cr-Mn-Ti gear steel. *Steel Res. Int.* **2019**, *90*, 1800332. [[CrossRef](#)]
23. Kong, W.D.; Zhang, D.K.; Tao, Q.; Chen, K.; Wang, J.; Wang, S.J. Wear properties of the deep gradient wear-resistant layer applied to 20CrMnTi gear steel. *Wear* **2019**, *424–425*, 216–222. [[CrossRef](#)]
24. Rudenko, S.P.; Val'ko, A.L. Contact fatigue resistance of carburized gears from chromium-nickel steels. *Met. Sci. Heat Treat.* **2017**, *59*, 60–64. [[CrossRef](#)]
25. Li, Y.; Cheng, G.G.; Lu, J.L.; Sun, J. The effect of TiN precipitated particles on the austenite grain and hardenability of 20CrMnTi gear steel. *Ironmak. Steelmak.* **2022**, *49*, 940–953. [[CrossRef](#)]
26. Zhang, Q.X.; Yuan, Q.; Wang, Z.T.; Qiao, W.W.; Xu, G. Enhanced mechanical properties in a low-carbon ultrafine grain steel by niobium addition. *Metall. Mater. Trans. A* **2021**, *52*, 5123–5132. [[CrossRef](#)]
27. Zhang, Q.X.; Yuan, Q.; Wang, Z.T.; Qiao, W.W.; Xu, G. Enhanced thermal stability of the low-carbon ultrafine grain steel with nanoprecipitates. *Steel Res. Int.* **2022**, *93*, 2100320. [[CrossRef](#)]
28. Tang, E.; Yuan, Q.; Zhang, R.; Zhang, Z.C.; Mo, J.X.; Liang, W.; Xu, G. On the grain coarsening behavior of 20CrMnTi gear steel during pseudo carburizing: A comparison of Nb-Ti-Mo versus Ti-Mo microalloyed steel. *Mater. Charact.* **2023**, *203*, 113138. [[CrossRef](#)]
29. Yuan, Q.; Ren, J.; Mo, J.X.; Zhang, Z.C.; Tang, E.; Xu, G.; Xue, Z.L. Effects of rapid heating on the phase transformation and grain refinement of a low-carbon microalloyed steel. *J. Mater. Res. Technol.* **2023**, *23*, 3756–3771. [[CrossRef](#)]
30. Gladman, T. *The Physical Metallurgy of Microalloyed Steels*; The Institute of Materials: London, UK, 1997.

Disclaimer/Publisher's Note: The statements, opinions and data contained in all publications are solely those of the individual author(s) and contributor(s) and not of MDPI and/or the editor(s). MDPI and/or the editor(s) disclaim responsibility for any injury to people or property resulting from any ideas, methods, instructions or products referred to in the content.